Marine Geophysical Research (2023) 44:15
https://doi.org/10.1007/s11001-023-09524-1

ORIGINAL RESEARCH PAPER

Joint elastic-electrical effective medium modeling for improved hydrate quantification

Haojie Pan[1] · Hongbing Li[2] · Jiajia Zhang[3] · Shengjuan Cai[4] · Zhixian Gui[1] · Miao Du[1]

Received: 1 January 2023 / Accepted: 2 May 2023 / Published online: 12 May 2023

Abstract

The occurrence of gas hydrates significantly alters the elastic and electrical responses of the host sediments. It is expected that joint inversion of the elastic and electrical data will provide a more accurate assessment of hydrate saturation. However, the unified relationship between hydrate saturation and the joint elastic and electrical properties of hydrate-bearing sediments, which is the key to successful evaluation of hydrate resources, has yet to be fully established. We develop a consistent joint elastic-electrical effective medium modeling framework for gas hydrate-bearing sediments. Comparison of the modeling results with available experimental data confirms the feasibility of the joint modeling approach for characterizing the elastic and electrical behaviors of pore-filling hydrate-bearing sediments. Based on the grid searching algorithm, a joint elastic-electrical inversion strategy is proposed to estimate the hydrate saturation from acoustic velocity and resistivity logs acquired at two marine hydrate sites: Hole U1328C in the northern Cascadia margin and Hole GC955H in the continental slope of the northern Gulf of Mexico. The hydrate saturations estimated from a combination of the P-wave velocity and resistivity at the chosen well sites (~5.93% at Site U1328C and ~47.1% at Site GC955H) are in good agreement with the references based on Archie's equation and its modified form and are more accurate than those interpreted from individual P-wave velocity (~9.01% at Site U1328C and ~45.3% at Site GC955H) and electrical resistivity (~10.35% at Site U1328C and ~54.4% at Site GC955H) data, validating the effectiveness of the joint elastic-electrical inversion approach.

Keywords Rock physics · Effective medium models · Joint elastic-electrical properties · Joint inversion · Hydrate saturation

✉ Hongbing Li
hbingli@petrochina.com.cn

Haojie Pan
panhaojie88@163.com

Jiajia Zhang
zhangjj@upc.edu.cn

Shengjuan Cai
s.cai20@imperical.ac.uk

Zhixian Gui
gyy68@126.com

Miao Du
18827080330@163.com

[1] College of Geophysics and Petroleum Resources, Yangtze University, Wuhan 430100, China

[2] Department of Geophysics, Research Institute of Petroleum Exploration and Development, Beijing 100083, China

[3] School of Geosciences, China University of Petroleum (East China), Qingdao 266580, China

[4] Resource Geophysics Academy, Imperial College London, London SW7 2BP, UK

Introduction

Gas hydrates are of widespread occurrence in continental margin sediments and beneath terrestrial permafrost regions (Kvenvolden 1993). They are considered to be an alternative energy source (Boswell and Collett 2011) and play pivotal roles in climate change and seafloor stability (Archer 2007; Sultan et al. 2004). For these reasons, accurate estimation of the amount and distribution of gas hydrates is of great significance for evaluating the resource potential and environmental implications. In general, the presence of gas hydrates often increases the elastic velocity and electrical resistivity of the host sediments. These anomalies provide an important basis for quantifying hydrates using well logs, seismic, and controlled source electromagnetic (CSEM) surveys (Ellis 2008; Goswami et al. 2015; Pan et al. 2019; Liu et al. 2020). However, the interpretation of a single type of geophysical observation data often suffers from non-uniqueness and thus provides quite different hydrate saturation estimates due to imperfect measurements, insufficient theory development,

and immature quantification methods (Cook and Waite 2018; Haines et al. 2022). Thus, a joint analysis of elastic and electrical data is necessary to improve hydrate assessment by providing complementary constraints on the rock properties.

Great efforts have been made to quantify gas hydrates through joint inversion of elastic and electrical properties (Lee 2002; Sava et al. 2011; Lee and Collett 2012; Pan et al. 2019; Liu et al. 2020; Pandey and Sain 2022). Most of these joint inversion methods involve independent elastic and electrical models that relate hydrate saturation separately to the acoustic velocity and electrical resistivity. Unfortunately, these models allow for different pore-scale interactions and microstructures, such as hydrate morphology, pore structure, and rock configuration (Archie 1942; Dvorkin and Nur 1996; Helgerud et al. 1999; Lee and Waite 2008), and may be inconsistent with each other due to certain specific assumptions and restrictions. Moreover, they are often implemented separately in joint quantification, greatly increasing the uncertainty of the hydrate saturation estimate (Wu and Grana 2017). As a consequence, successful joint quantification requires a unique theoretical modeling scheme that links the joint elastic-electrical behaviors to a common set of rock components and microstructural configuration.

Inclusion-based effective medium theories have been widely used to model the elastic and electrical responses of sedimentary rocks and have achieved great success (Jakobsen et al. 2000; Chand et al. 2006; Ghosh et al. 2010; Han et al. 2011; Jensen et al. 2013; Han et al. 2016; Amalokwu et al. 2019; Han et al. 2022). Among them, the first principle-based self-consistent approximation (SCA) and the differential effective medium (DEM) model are two of the most commonly used theories for independent elastic and electrical calculations (Berryman 1995; Mavko et al. 2009). SCA models keep the microstructure of the rocks consistent but fail to generate a bi-connected medium over a wide range of volume fractions (Jakobsen et al. 2000). In comparison, DEM models require the addition of an insulating solid matrix to the conducting fluid background for the electrical modeling but the addition of pore inclusions to the sediment matrix for the elastic modeling (Sheng 1991; Berryman 1995; Cosenza et al. 2003; Gelius and Wang 2008; Markov et al. 2005). As a result, neither SCA nor DEM models can independently model the elastic and electrical responses of a bi-connected composite at any volume fraction. To capture the joint elastic-electrical behaviors of shaly sandstones, Han et al. (2011) developed a three-component elastic and electrical SCA-DEM effective medium model by incorporating the quartz, clay, and brine. Using the baseline model of Han et al. (2011), Attias et al. (2020) further established a three-component joint elastic-electrical SCA-DEM model for clay-rich hydrate reservoirs and quantified the hydrate saturation via semi-quantitative analysis of the inverted seismic velocity and CSEM-derived resistivity. However, these models simplify the considerations of the mineral composition, pore fluids, microstructures, and hydrate distribution and thus fail to quantify the gas hydrates accurately.

This study aims to establish a unified joint elastic-electrical effective medium model for hydrate-bearing sediments and propose a joint inversion scheme for improving the accuracy of hydrate saturation estimate. We first construct a four-component joint elastic-electrical model based on three rounds of a two-phase SCA-DEM model for pore-filling hydrate-bearing sediments with a consistent microstructure. Then, we test the validity of the models by comparing the joint elastic-electrical modeling results with the experimental data. Finally, the calibrated modeling procedure combined with the grid searching method is applied to estimate the hydrate saturation from well-log data at two marine hydrate sites.

Methodology

In this section, the two-phase elastic and electrical SCA-DEM models are first described as they provide a theoretical basis for the joint elastic-electrical simulations. The two-phase models are then tested using experimental data and are compared with other theoretical models. Based on the two-phase SCA-DEM model, a unified modeling workflow for the joint elastic-electrical properties is developed by successively incorporating hydrates, water, clay, and quartz. These components have different bulk and shear moduli and densities summarized in Table 1. Finally, a joint elastic-electrical inversion approach based on grid searching method is proposed to obtain the optimal solution.

Table 1 Physical properties of the constituents used in the modeling

Medium	Bulk modulus (GPa)	Shear modulus (GPa)	Density (g/cm^3)	Resistivity (Ωm)	References
Quartz	36.6	45	2.65	10^5	Han et al. (2011)
Clay	20.9	6.85	2.58	33	Attias et al. (2020)
Hydrate	6.41	2.54	0.91	200	Pan et al. (2019); Attias et al. (2020)
Water	2.25	0	1.03	0.082	Pan et al. (2019); and Computed resistivity

Two-phase effective medium models

Elastic SCA-DEM model

The SCA model treats all of the rock components equally without a preferential host medium. The bulk and shear moduli of the two-phase composite at the critical concentration (ϕ_c, a volumetric proportion that keeps the two phases connected) are expressed as (Mukerji et al. 1995):

$$(1-\phi_c)(K_1-K_{SCA})P^{*1}+\phi_c(K_2-K_{SCA})P^{*2}=0, \quad (1)$$

$$(1-\phi_c)(G_1-G_{SCA})Q^{*1}+\phi_c(G_2-G_{SCA})Q^{*2}=0, \quad (2)$$

where the subscripts 1 and 2 denote the first and second components, respectively; K and G are the bulk and shear moduli, respectively; P^* and Q^* are the geometrical factors, respectively; and K_{SCA} and G_{SCA} are the effective self-consistent bulk and shear moduli, respectively.

The above calculated elastic moduli at the critical concentration are then used as the elastic moduli of the background medium in the DEM model. For rocks with volume fractions of greater and less than the critical concentration, the first component or second component with an infinitesimal volume is added to the background using the DEM models until the desired volume fraction of each phase is attained. According to the DEM theory, the bulk and shear moduli at any concentration can be calculated as follows (Berryman 1995):

$$dK_{DEM}(v_i)=\frac{(K_i-K_{DEM}(v_i))P^{*i}}{1-v_i}dv_i, \quad (3)$$

$$dG_{DEM}(v_i)=\frac{(G_i-G_{DEM}(v_i))Q^{*i}}{1-v_i}dv_i, \quad (4)$$

where the boundary conditions are $K_{DEM}(v_i=\phi_c)=K_{SCA}$ and $G_{DEM}(v_i=\phi_c)=G_{SCA}$, K_i and G_i are the bulk and shear moduli of the inclusion, respectively; v_i is the volume fraction of the inclusion; P^{*i} and Q^{*i} are the geometric factors of the inclusion; and K_{DEM} and G_{DEM} are the bulk and shear moduli of the two-phase composite, respectively.

Figure 1 compares several elastic effective medium models with a set of published laboratory data collected for 27 sandstones with porosities of 9–29% at a differential pressure of 8 MPa (Han 2010). Here, the clean sandstones are assumed to be composed of quartz grains and water-filled pores. The critical concentration, the aspect ratios of grains and pores are set to 0.4, 1.0 and 0.2, respectively. As can be seen, the elastic moduli calculated using all three models are well within the Hashin–Shtrikman (HS) bounds. However, the SCA model predictions are exactly the same as those of the lower HS bound for porosities of > 55%, and the DEM model overestimates the elastic properties at porosities of > 15%. Whereas, the SCA-DEM model gives the best predictions of bulk and shear moduli compared to the measurements, confirming its advantage over both the SCA and DEM models in capturing the elastic responses.

Electrical SCA-DEM model

Similarly, the electrical SCA model is employed to calculate the electrical conductivity of the two-phase composite at the critical concentration. The expression is as follows (Mavko et al. 2009):

$$(1-\phi_c)(\sigma_1-\sigma_{SCA})R^{*1}+\phi_c(\sigma_2-\sigma_{SCA})R^{*2}=0, \quad (5)$$

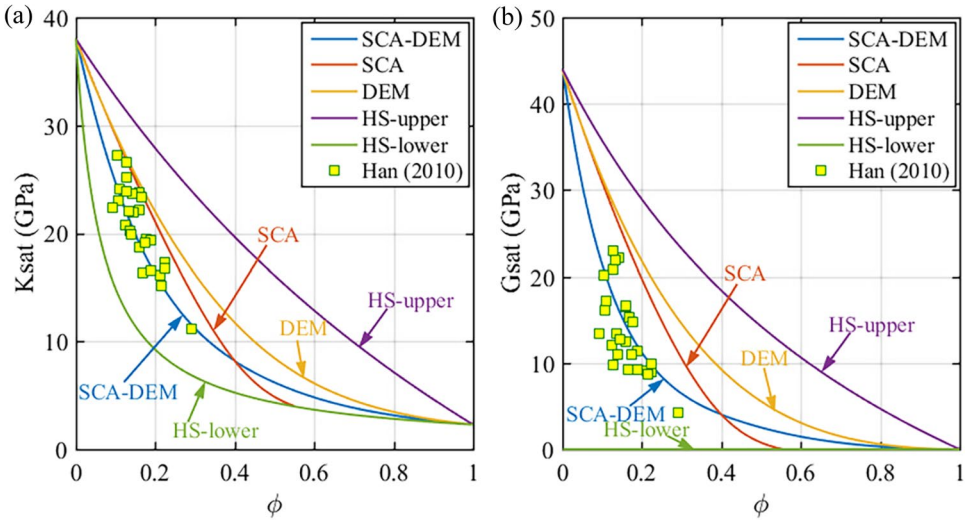

Fig. 1 The modeled **a** bulk (K_{sat}) and **b** shear (G_{sat}) moduli of saturated rock as a function of porosity for the elastic SCA, DEM, and SCA-DEM models and the HS bounds. The laboratory data utilized for comparison are from Han (2010)

where σ is the electrical conductivity, and R^* is the effective depolarization factor.

Then, the DEM model is used to compute the electrical conductivity by replacing the background material with the inclusion. This procedure is repeated until the final volume fraction of the inclusion is reached. The DEM model expression for the electrical conductivity at any concentration is as follows (Mavko et al. 2009):

$$d\sigma_{DEM}(v_i) = \frac{(\sigma_i - \sigma_{DEM}(v_i))R^{*i}}{1 - v_i} dv_i, \tag{6}$$

where the initial condition is $\sigma_{DEM}(v_i = \phi_c) = \sigma_{SCA}$, σ_i and R^{*i} are the conductivity and the depolarization factor of the inclusion, respectively; and σ_{DEM} is the conductivity of the two-phase composite.

Figure 2 compares several electrical models with laboratory measurements. As expected, all three models fall within the resistive and conductive HS bounds, confirming their validity in modeling the electrical response. However, these models predict quite different dependences of the electrical resistivity on the porosity. By comparing with laboratory measurements, we find that the DEM model provides good predictions of the electrical resistivity of the water-saturated sandstones at moderate porosities, but it underestimates the electrical resistivity at lower porosities. The SCA model largely overestimates the electrical resistivity of the composites at porosities of < 40%. In comparison, the SCA-DEM model predictions match the laboratory data well, validating its superiority in modeling the electrical resistivity of a two-phase medium compared to independent application of the SCA or DEM models.

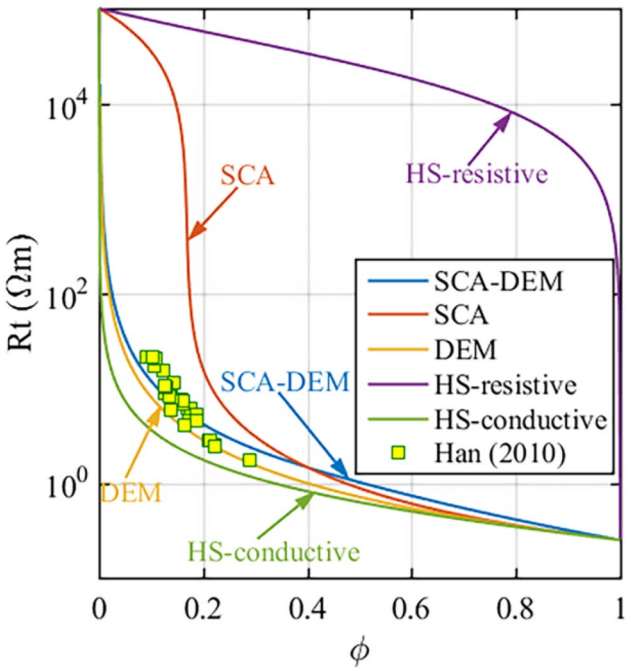

Fig. 2 The modeled electrical resistivity of saturated rock (R_t) as a function of the porosity using the electrical SCA, DEM, and SCA-DEM models and the HS bounds. The laboratory data utilized for comparison are from Han (2010)

Joint elastic-electrical modeling

Since the DEM models preserve the connectivity of the starting medium produced by the SCA models at porosities of 40–60%, the SCA-DEM models solve the adding order problem of the DEM model and overcome the disadvantage of the SCA model, i.e., both phases are only connected within a limited range of volumetric fractions. As a consequence, both the elastic and electrical SCA-DEM models provide reasonable predictions of the elastic moduli and resistivity of clean sandstones. As affected by the sediment characteristics, gas hydrates are often present in different types of sediments, ranging from coarse-grained sand-dominated layers to fine-grained clay-rich formations, each of which hosts a variety of hydrate morphologies, which occur as two basic types: grain-displacing and pore-filling. Since the SCA and DEM theories used here are isotropic formulations, we ignore the anisotropic behaviors of hydrate reservoirs and assume that the gas hydrates reside in the pore spaces. Based on the work of Han et al. (2011) and Attias et al. (2019), a novel four-component elastic-electrical SCA-DEM effective medium model that resembles the microstructural distribution of quartz, clay, water, and hydrates, is developed to better characterize pore-filling hydrate reservoirs.

Figure 3 illustrates the detailed modeling workflow of the joint elastic-electrical SCA-DEM model. First, a two-phase fluid mixture composed of water and pore-filling hydrates at a critical concentration is created using the SCA model. Then, the DEM model is used to obtain the effective medium at any concentration by replacing the fluid mixture with water or pore-filling hydrates. Next, the resulting fluid mixture is combined with clay with the same aspect ratio as those of ellipsoidal pores using the two-phase SCA-DEM models again to achieve the effective properties of the three-component clay-fluid mixture. Finally, the remaining spherical quartz is included in the aggregated clay-water-hydrate composite using the two-phase SCA-DEM models for a third time to determine the elastic and electrical properties of the fully connected pore-filling hydrate-bearing sediments. In this modeling procedure, the volume fractions of water (f_w), pore-filling hydrates (f_h), clay (f_c) and quartz (f_q) are given by $f_w = \phi(1 - S_h)$, $f_h = \phi S_h$, $f_c = (1 - \phi)V_c$ and $f_q = (1 - \phi)(1 - V_c)$, respectively, where ϕ is the porosity, S_h is the hydrate saturation, and V_c is the clay content.

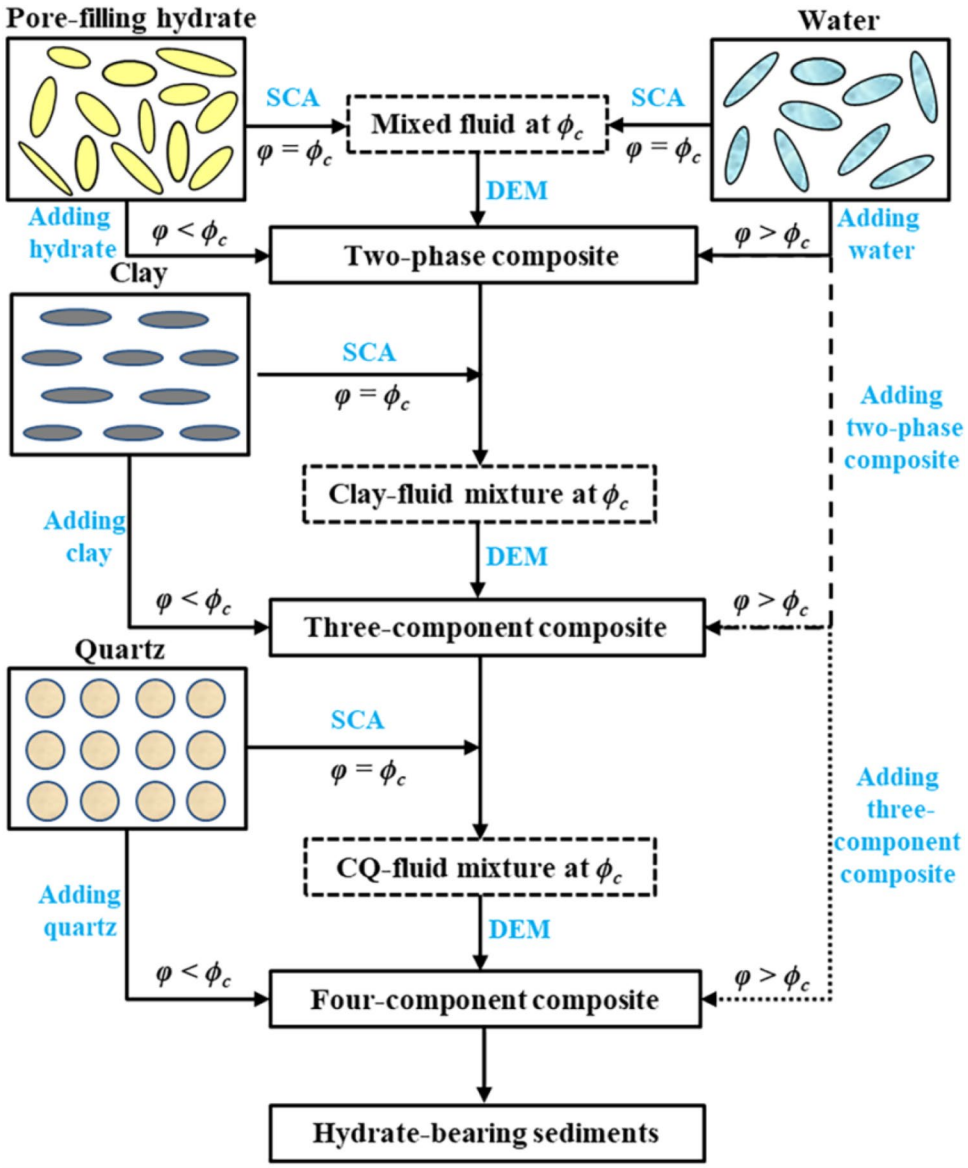

Fig. 3 Workflow for modeling the elastic and electrical properties of pore-filling hydrate reservoirs based on three rounds of a two-phase SCA-DEM model. CQ denotes a mixture of clay and quartz

Joint elastic-electrical inversion

Based on the joint elastic-electrical modeling framework, hydrate saturation can be determined from the measured acoustic velocity and resistivity using iterative sampling/optimization technique. Here, an enumeration method, grid searching algorithm, is used to find an optimal solution by minimizing the mismatch between the model predictions and measured data. Given the observed elastic and electrical data, the hydrate saturation can be inverted by solving a nonlinear problem for minimization of cost function:

$$J(S_h) = \min\left[\eta\left(\frac{V_p^{obs} - V_p^{cal}(S_h)}{V_p^{obs}}\right)^2 + (1-\eta)\left(\frac{R_t^{obs} - R_t^{cal}(S_h)}{R_t^{obs}}\right)^2\right] \quad (7)$$

where V_p^{obs} and R_t^{obs} are the measured P-wave velocity and resistivity, respectively; V_p^{cal} and R_t^{cal} are the P-wave velocity and resistivity calculated using the joint elastic-electrical modeling scheme, respectively; and η is defined as the weighting factor ranging from 0 to 1, which controls the relative importance of each data in the inversion procedure. Here, $\eta = 0$, $\eta = 1$, and $\eta = 0.5$, respectively, represent the individual resistivity, individual P-wave velocity, and joint elastic-electrical inversion strategies.

The detailed inversion procedure for predicting hydrate saturation is shown in Fig. 4. The values of P-wave velocity and resistivity are computed with the joint elastic-electrical model from the interpreted clay content and porosity for the preset value range of hydrate saturation. Then, the objective function can be evaluated using Eq. (7). The

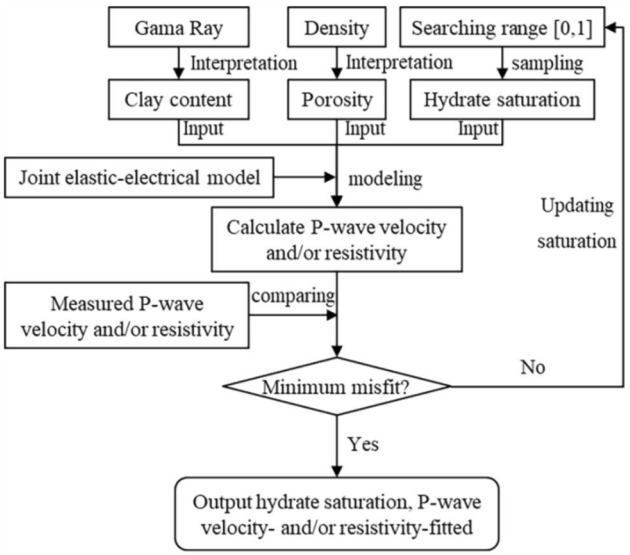

Fig. 4 Flow chart of the hydrate saturation estimation from P-wave velocity and/or resistivity data using the grid searching method

minimum misfit between the measured elastic and electrical properties and those computed from the joint elastic-electrical model provides the best solution of hydrate saturation. By repeating the procedure for each depth, the hydrate saturation can be estimated for the whole interval of interest.

Results

Model validation with laboratory data

We verified the proposed joint elastic-electrical modeling approach using the experimental data acquired by Ren et al. (2010), who simultaneously measured the acoustic velocity and electrical resistivity of artificial hydrate sand samples during hydrate formation. The laboratory experiments were conducted at 5 °C and a methane pore pressure of 16 MPa. The initial porosity is 34.2%, and the aspect ratios of the sand grains and pores are assumed to be 1.0 and 0.2, respectively.

Figure 5 compares the experimental measurements with the model predictions for hydrate saturations ranging from 0 to 1.0. It can be seen that the P-wave velocity and resistivity both increase with increasing hydrate saturation and decrease with increasing critical concentration. In addition, the trend generated using the proposed modeling strategy with a critical concentration value of 0.6 shows a good fit to most of the measured data. However, it significantly underestimates the P-wave velocity at hydrate saturations of > 50% and the resistivity at hydrate saturations of > 30%. This underestimation is primarily attributed to the transition of the hydrate morphology from pore-filling to load-bearing as the hydrate saturation increases. The explanation for this phenomenon is that hydrates tend to float in the pore space at a low to moderate saturation (roughly 25–40%, and increasing with grain size), while they bridge the sediment grains and block the pore throats at higher saturations, significantly increasing P-wave velocity and resistivity. From this comparison, we conclude that the proposed model not only captures the joint elastic-electrical properties of pore-filling hydrate-bearing sediments but also provides insights into the evolution pattern of hydrate morphology through the joint analysis of the elastic and electrical responses.

Gas hydrate quantification

To assess the performance of the four-component SCA-DEM model in quantifying gas hydrates, we chose two sets of well-log measurements for Hole U1328C in the northern Cascadia margin, and Hole Green Canyon 955H (GC955H)

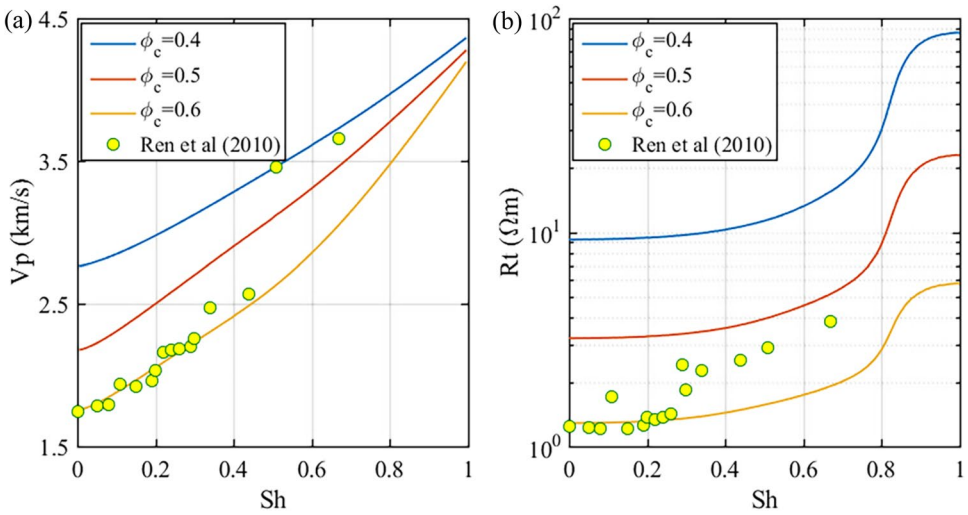

Fig. 5 Comparison of the measured P-wave velocity (V_p) and resistivity (R_t) with the model estimates as a function of the hydrate saturation for different critical concentrations. The laboratory measurements denoted as yellow circles are from Ren et al. (2010)

in the continental slope of the northern Gulf of Mexico. Well-log data, such as the P-wave velocity, resistivity, density, and Gama ray (GR) logs, were collected at both sites (Riedel et al. 2006; Lee and Collett 2012). The quality of the well-log data evaluated using the caliper log is generally good throughout the intervals of interest, from 80 to 219 m below seafloor (mbsf) in Hole U1328C and from 413 to 440 mbsf in Hole GC955H. Based on analysis of the well-log data and observations of core samples, we find that the sediment matrix primarily consists of sand and clay, and the pore fluid is a mixture of hydrates and water. For simplicity, we assumed that the clay had the same low aspect ratio as the pore spaces while the quartz grains were assigned with aspect ratios equal to unity. In addition, the clay content and porosity were derived from the GR and density logs, respectively, instead of setting them as constants. Typically, the hydrate saturations estimated via quantitative degassing of pressure core samples and nuclear magnetic resonance (NMR)-density porosity analysis are relatively more precise and are often used as ground truth data for assessing the accuracy of other methods. As no NMR logs and pressure cores were collected within the studied intervals for the target areas, the hydrate saturation calculated from the resistivity log using Archie's equation or its modified form (Archie 1942) was taken as the reference. Finally, the joint elastic-electrical inversion based on a grid searching approach was applied to estimate the gas hydrate saturation from the P-wave velocity and/or resistivity data.

Site U1328C in the northern Cascadia margin

During Expedition 311 of the Integrated Ocean Drilling Program (IODP), Hole U1328C was drilled at a cold vent in the northern Cascadia margin offshore of Vancouver Island. The vertical seismic blanking, well logs, and core samples show clear evidence of the presence of gas hydrates within the alternating relatively coarser-grained silty sand and sand layers. Additionally, previous studies of this site have indicated that most of the gas hydrates are located in the pore spaces, and small amounts fill veins and fractures (Pan et al. 2019; Holland et al. 2008). Thus, by assuming the isotropic behavior of pore-filling hydrate-bearing sediments, we assessed the hydrate saturation based on the well-log data using the proposed joint inversion method.

Before estimating the hydrate saturation, additional parameters, such as the critical concentration and aspect ratios of the pores (PAR) and grains (GAR), need to be determined. Figure 6 compares the P-wave velocity and resistivity calculated using the four-component SCA-DEM model with the well-log data for the hydrate-free intervals. A critical concentration of 0.6 and a pore aspect ratio of 0.2 produce reasonable fits between the measured P-wave velocity and resistivity and the predictions for water-saturated sediments. Therefore, the calibrated model can be used to predict the hydrate saturation from the acoustic velocity and resistivity logs.

As shown in Fig. 7a and b, the P-wave velocity values jointly modeled using the four-component SCA-DEM model are the same as the observed values, whereas the values obtained using the individual models are overestimated in two intervals, 106.54–115.98 m and 118.12–127.87 m. Unlike the acoustic case, the resistivities obtained using both the individual and joint inversion strategies are almost identical to the measured resistivity when the resistivity is greater than 1.05 Ωm, but they are slightly higher than the observed data when the resistivity is less than 1.05 Ωm. Overall, the calculated P-wave velocity and resistivity agree well with the measured values, especially in terms of maintaining a general variation trend. To account for the effect of the clay on the electrical resistivity, a modified Archie's equation (Sava and Hardage 2007) with a tortuosity factor of 1.0, a cementation

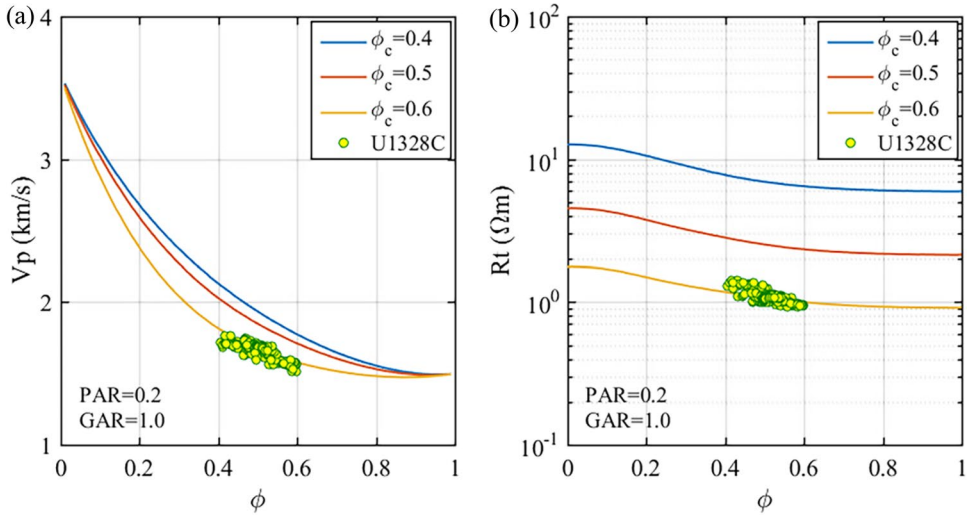

Fig. 6 Plots of **a** P-wave velocity and **b** resistivity versus porosity for different critical concentrations. The superimposed data points are the well-log data for Hole U1328C in the northern Cascadia margin

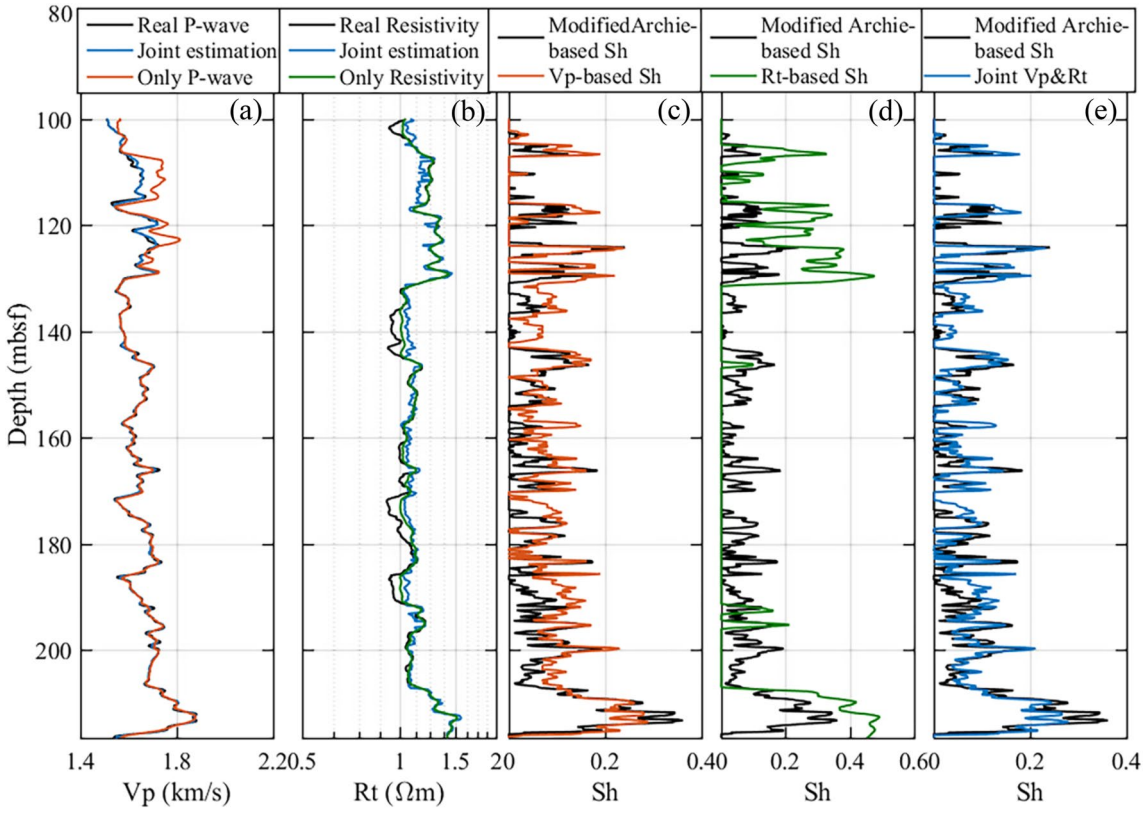

Fig. 7 Inversion results for Hole U1328C: **a** P-wave velocity, **b** resistivity, and **c**–**e** hydrate saturation. The measured data and modified Archie-based hydrate saturation are shown in black, the predictions obtained using the joint inversion are shown in blue, and those obtained using only the P-wave velocity and only the resistivity are shown in red and green, respectively. All log-based saturations are smoothed with a 5-point running average

exponent of 2.9, and a saturation exponent of 2.0 (Riedel et al. 2006), was used to obtained the reference data. Here, the connate water resistivity was determined using the formulas proposed by Fofonoff (1985) and by combining the depth-dependent salinity and formation temperature. Figure 7c–e compare the hydrate saturations estimated using only the P-wave velocity, only the resistivity, and both the P-wave velocity and the resistivity with the reference saturation. In Fig. 7c, the P-wave velocity-based estimate ranges from 0 to 32.5%, with an average saturation of 9.01%. It is slightly overestimated at low hydrate saturations (< 10%) and is close to the reference value at relatively high hydrate saturations. As shown in Fig. 7d, the estimation based on the resistivity data has an average value of 10.35%, but it locally exceeds 49.2% and is negligible in the low-resistivity interval at depths of 132–207 mbsf. It differs by a maximum of 30% in the upper (< 132 mbsf) and lower (> 207 mbsf) high-resistivity (> 1.1 Ωm) layers. This large discrepancy is most likely caused by the oriented clay minerals and hydrate fractures. In addition, the constant resistivity of the pore water in the four-component SCA-DEM model also adds to the inconsistency. In contrast, the joint inversion result in Fig. 7e is in good agreement with the Archie-based reference data, with an average hydrate saturation of 5.93% and a maximum saturation of up to 28% at depths of 80–219 mbsf.

To further evaluate the accuracies of the hydrate saturation estimates, we calculated the correlation coefficients and the root mean square errors for the results of the individual and joint inversion strategies within the hydrate intervals (Fig. 8). The correlation coefficients and root mean square errors of the three estimates are 85.87% and 0.0025 for the P-wave velocity alone, 59% and 0.0287 for the resistivity alone, and 92.97% and 0.00068 for the joint interpretation, respectively. Based on the above statistical analysis, we conclude that the estimate based on the P-wave velocity is better than that based on the resistivity, and the joint elastic-electrical interpretation is more accurate than those obtained using the P-wave velocity alone and using the resistivity alone. The accuracy improvement of the joint elastic-electrical estimation is mainly due to the fact that the joint use of the elastic and electrical properties provides complementary but independent constraints on the estimate, thus alleviating the interpretation ambiguity.

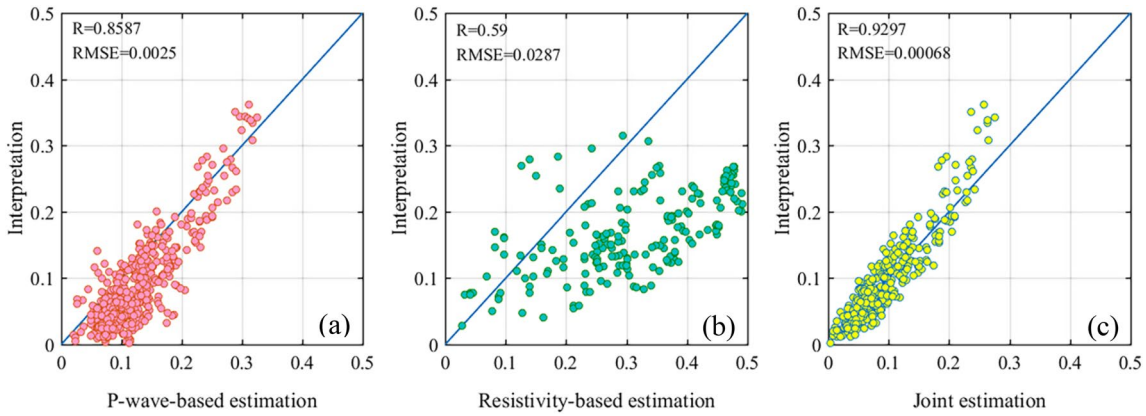

Fig. 8 Comparison of hydrate saturations estimated using **a** only the P-wave velocity, **b** only the resistivity, and **c** the joint elastic-electrical properties and the modified Archie-based reference data for Hole U1328C. R and RMSE denote the correlation coefficient and root mean square error, respectively

Site GC955H in the northern Gulf of Mexico

During the spring of 2009, the Gulf of Mexico Gas Hydrate Joint Industry Project conducted its Leg II operation and collected logging-while-drilling (LWD) data at three sites on the continental slope of the northern Gulf of Mexico. Analysis of the well-log data for Hole GC955H revealed that the hydrates fill the fractures in the clay-bearing zone (183–366 mbsf) and occupy the pore spaces in the sand zone (413–440 mbsf) (Lee and Collett 2012; Cook and Waite 2018). Here, we focused on quantifying the pore-filling hydrates within the sand layers using the proposed joint elastic-electrical modeling scheme.

Similarly, a comparison of the modeled and measured P-wave velocity and resistivity data for the non-hydrate intervals was used to calibrate the free parameters in the proposed model. Optimization of the calculated elastic and electrical responses of the water-bearing sediments and the actual data above the target intervals yielded a critical concentration of 0.56 and a pore aspect ratio of 0.4 (Fig. 9). The calibrated model increases the confidence of the predicted hydrate saturation.

Figure 10a and b show the measured and inverted P-wave velocity and resistivity data for the hydrate-bearing sediments. As can be seen, the individually modeled P-wave velocity is identical to the actual value, whereas the jointly modeled P-wave velocity has some differences but follows the overall variation trend of the measured data. In contrast, both the jointly and individually modeled resistivity fit the measured data quite well. Figure 10c–e show a comparison of the gas hydrate saturation estimated using the P-wave velocity, electrical resistivity, and both properties using the four-component SCA-DEM model. Due to a lack of core data and NMR log, the reference saturation was calculated from the electrical resistivity using Archie's equation. For the Archie parameters, we used with a tortuosity factor of

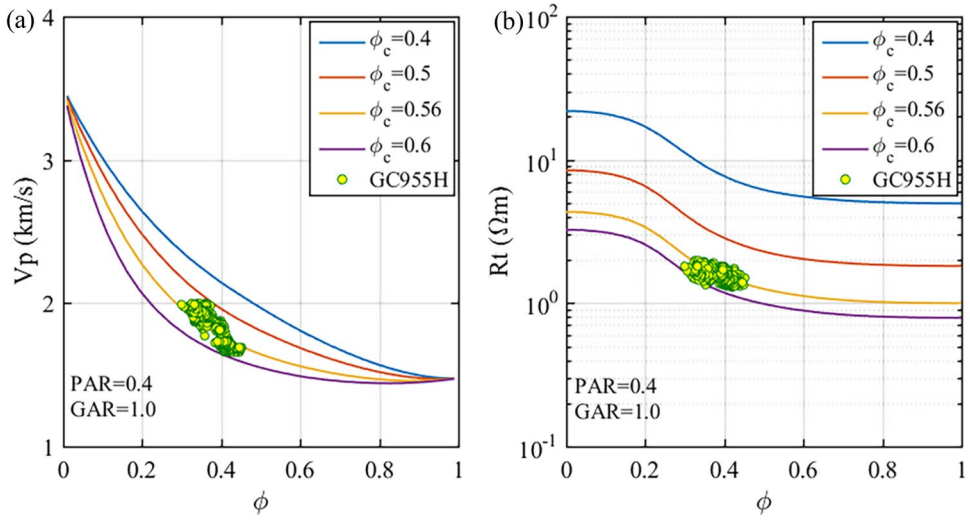

Fig. 9 Plots of **a** P-wave velocity and **b** resistivity versus porosity for different critical concentrations. The superimposed data points are the well-log data for Hole GC955H in the continental margin of the northern Gulf of Mexico

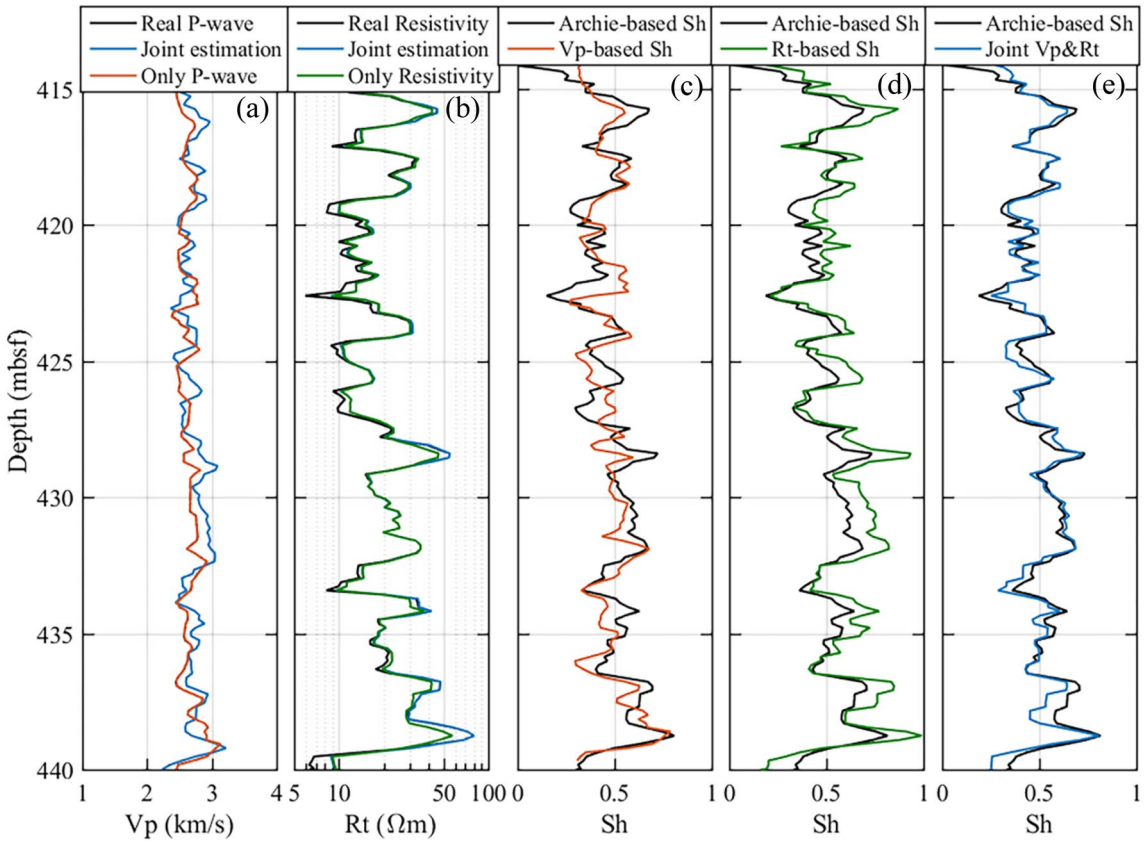

Fig. 10 Inversion results for Hole GC955H: **a** P-wave velocity, **b** resistivity, and **c**–**e** hydrate saturation. The measured data and Archie-based hydrate saturation are shown in black, the predictions obtained via joint inversion are shown in blue, and those obtained using only the P-wave velocity and only the resistivity are shown in red and green, respectively. All log-based saturations are smoothed with a 5-point running average

1.0, a cementation exponent of 1.8, and a saturation exponent of 2.0 as suggested by Lee et al. (2012). It can be seen that different methods and different datasets exhibit more or less the same hydrate saturation variation trend. For the velocity-based prediction, the hydrate saturation is as high as 72.9%, with an average value of 45.3%, which is slightly underestimated compared with the reference value. In comparison, the resistivity-based saturation estimate, with an average value of 54.4% and a maximum value of 98.9%, is comparable to the Archie-based reference value in the non-hydrate intervals, but it overestimates the value in several hydrate-bearing intervals. By comparing the two individual estimates, the possible dissociation of the methane hydrates during the drilling activity might be responsible for their large discrepancy. This is mainly because the existence of free gas increases the resistivity and sharply decreases the P-wave velocity. The hydrate saturation estimate based on the joint inversion (0–80.8% in the pore space, average of 47.1%) is quite consistent with the reference value overall.

Figure 11 compares the results of the hydrate saturation estimates obtained using different methods. The hydrate saturation estimated using only the P-wave velocity exhibits a large amount of scattering around a 45° line, with a correlation coefficient of 69.65% and a root mean square error of 0.0084. In addition to free gas, the difference in the resolution (or the depth of investigation) of the acoustic and resistivity logging tools and the depth-shift problem may be responsible for this data scattering. In comparison, the resistivity-based estimate deviates from a 45° line, with a correlation coefficient of 95.04% and a root mean square error of 0.0083, indicating overestimation at higher saturations. For the joint elastic-electrical inversion, the good alignment of the data clusters along a 45° line, with a high correlation coefficient of 92.16% and a low root mean square error of 0.0023, which clearly suggests that the joint inversion achieves the better accuracy compared to other methods.

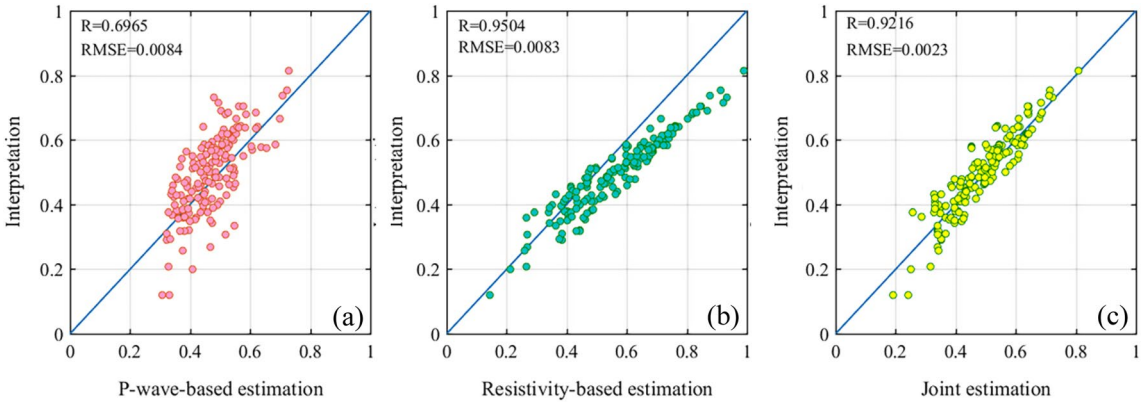

Fig. 11 Comparison of hydrate saturation estimates obtained using **a** only the P-wave velocity, **b** only the resistivity, and **c** the joint elastic-electrical properties and the Archie-based reference data for Hole GC955H

Discussion

In this study, we developed a joint elastic-electrical SCA-DEM modeling scheme for hydrate-bearing sediments. This method requires that all of the components of the sedimentary rocks be fully connected and randomly distributed. In addition, it includes a consistent microstructural description of the elastic and electrical responses and uses a common set of additional parameters. Moreover, the quartz grains are assigned a high aspect ratio of close to unity, while the clay minerals are assumed to have the same low aspect ratio as the pores. More importantly, it provides flexibility for modeling the elastic and electrical responses individually or jointly. By replacing the water phase with a free gas–water mixture, the joint elastic-electrical modeling approach can be used to predict the elastic and electrical responses of the host sediments coexisting with the free gas and hydrates. In addition to modeling the elastic and electrical responses, the proposed four-component SCA-DEM model can also be extended to mimic thermal conductivity and dielectric permittivity. However, it has limitations due to the approximations and assumptions that we made. For example, the proposed model assumes that the gas hydrates are present in the pore spaces. However, gas hydrates often takes on complex morphologies instead of a single form in the host sediments, which has been proven through extensive field studies and laboratory observations. For example, gas hydrates have been found to occur as a combined morphology of cementing and pore-filling under the excess-gas condition (Priest et al. 2005; Hu et al. 2014; Dugarov et al. 2019; Pan et al. 2020), while they have been found to exhibit mixed pore-filling, load-bearing, and/or fracture-filling morphologies in natural environments (Holland et al. 2008; Yoneda et al. 2018). In addition, our modeling scheme only holds true for isotropic hydrate reservoirs. However, in reality, most marine sediments are rich in clay minerals that exhibit inherent anisotropy due to the orientation of the clay platelets (Ghosh and Ojha 2021). The aligned fractures or veins in fine-grained sediments also create a high degree of anisotropy (Lee and Collett 2009; Riedel et al. 2014). Therefore, the proposed isotropic joint elastic-electrical modeling scheme needs to be further improved by considering the complex hydrate morphologies and the anisotropy caused by fractures and clay minerals.

We also used the established joint elastic-electrical inversion strategy to predict the hydrate saturation from P-wave velocity and resistivity logs at two marine sites where hydrate morphology is dominated by pore-filling. The comparisons of the estimates and the reference data (Figs. 8 and 11) suggest that the joint elastic-electrical inversion scheme improves the accuracy of the hydrate saturation estimate to a large degree. Whereas, the hydrate saturations estimated using only the P-wave velocity and only the electrical resistivity differ from each other and exhibit variability at these two sites, especially at Site U1328C. In addition to the data quality, the differences in the hydrate saturation estimates can be attributed to several other factors, including the different vertical resolutions of logging tools, depth-shift problem, the anisotropic hydrate distribution and the coexistence of free gas and hydrates. More specifically, the hydrate saturation is overestimated based on both properties when the anisotropic nature of the hydrate reservoirs is ignored, while it is underestimated based on the acoustic velocity and is overestimated based on the electrical resistivity when the presence of free gas is ignored. Moreover, an unreasonable choice of the pore water resistivity value may also cause the hydrate saturation estimated from the individual resistivity to differ for clay-rich sediments. Also, the introduction of free parameters (e.g., the critical concentration and pore aspect ratio) used in rock-physics modeling may introduce uncertainty into the estimation of the hydrate saturation. In this study, these additional parameters were calibrated

by fitting the model predictions to the elastic and electrical measurements for the non-hydrate reservoir intervals. Due to the lack of NMR logs and pressure core samples for the chosen sites, the hydrate saturation estimated using Archie's equation and its modified form was taken as the reference for assessing the accuracies of the different estimation methods. It should be pointed out that Archie's equation is designed for clean sandstones, and its accuracy is reduced when applied to clay-rich sediments. Therefore, Archie's equation was used for Hole GC955H, while a modified version was used for the clay-rich sediments in Hole U1328C. In addition, Archie's equation and its modified form are only valid for water-wetted rocks and are applicable for quantifying pore-filling hydrates because they are treated as part of the pore fluid and do not affect the water-wetted characteristics of the grain surface.

Hydrate quantification is an inverse procedure from geophysical measurements to hydrate content. To avoid suffering from local minima or relying on the starting model, a straightforward grid searching algorithm was used to find the optimal solution by fitting the theoretical data to the measured data. Unlike the gradient-based optimization, this method considers all possible solutions and requires extensive computations as it divides the entire value range of the unknown variable into uniform grids and evaluates the error function at each point. The accuracy of the estimation and computational efficiency are highly dependent on the grid spacing used. A smaller grid spacing can provide more accurate estimations, but at the expense of longer computational time. Since the total number of all the possible hydrate saturations, varying from 0 to 1.0 with a grid spacing of 0.01, is not very large, it enables us to achieve a fast and satisfactory estimation of hydrate saturation. However, for most large-scale geophysical inversion problems, it is impractical to use this enumeration method to solve the nonlinear high-dimensional problem. Another issue is the convergence of the grid searching-based joint inversion procedure. In Figs. 7 and 10, although the joint analysis of multiple geophysical observations could provide a significant improvement in the accuracy and reliability of inversion estimate, the differences between the model predictions and measured data for the joint inversion are larger than those for the individual inversion. It is of no surprise because the joint inversion of the elastic and electrical data for estimating hydrate saturation is to solve an overdetermined inverse problem, in which the number of data is barely more than that of unknown. Accordingly, it seems to be hard to achieve a balance between the inversion convergence and estimation accuracy using the grid searching method. Regarding the over-determined inversion problem, we suggest the use of iterative optimization or the appropriate selection of the weighting factor in the objective function to attain a quick and steady convergence to the optimum. Besides, the grid searching method fails to make a statistical evaluation of the result uncertainty. Therefore, the follow-up research will be placed on the joint inversion of elastic and electrical data for quantifying hydrate saturation and its uncertainty simultaneously under the framework of Bayesian theory.

Conclusions

Using a combination of the SCA and DEM models, we established a four-component joint elastic-electrical effective medium model for gas hydrate-bearing sediments. This model incorporates a consistent microstructural description of the elastic and electrical behaviors of a fully connected medium. When a reasonable critical concentration and reasonable grain and pore aspect ratios are used, the modeled P-wave velocity and electrical resistivity are in good agreement with available laboratory data for clean sandstones containing hydrates at low to moderate saturations, but they are much lower than the measured elastic and electrical properties at moderate to high hydrate saturations. The validation of the model not only demonstrates the capability of our modeling approach to capture the joint elastic-electrical properties of pore-filling hydrate-bearing sediments but also indicates the evolution of the hydrate morphology during hydrate formation. The proposed joint elastic-electrical modeling scheme combined with the grid search algorithm was used to quantify the hydrate saturation based on P-wave velocity and resistivity logs acquired at Site U1328C on the northern Cascadia margin and Site GC955H on the continental slope of the northern Gulf of Mexico. Compared with the predictions based on the individual properties, the hydrate saturations estimated through joint inversion are satisfactorily consistent with the reference values for these two marine sites. The discrepancy between the hydrate saturations calculated using the different measurements indicates that the alignment of the clay minerals, hydrate veins and/or fractures, and free gas have great influences on the elastic and electrical properties and hydrate saturation estimates. The developed joint elastic-electrical modeling and inversion methods are demonstrated to have a good performance in quantifying hydrates based on well-log data, and it can potentially improve the joint interpretation of seismic and CSEM surveys for better characterization of hydrate reservoirs.

Acknowledgements We are grateful to the scientists and personnel associated with IODP Expedition 311 and GOM JIP Leg II. Special appreciation is extended to Prof. Tongcheng Han for his helpful discussions and insights during development of the model. We would also like to thank the two anonymous reviewers for their constructive comments and suggestions that strengthen the paper.

Author contributions Not applicable.

Funding This work is supported by the National Natural Science Foundation of China (42104121), and Basic Research and Strategic Reserve Technology Funds for Affiliated Institutions of China National Petroleum Corporation (2018D-500811).

Data availability The well-log data used in the current study are freely available and accessible through the link https://mlp.ldeo.columbia.edu/logdb/scientific_ocean_drilling/.

Declarations

Conflict of interest The authors declare that they have no known competing financial interests or personal relationships that could have appeared to influence the work reported in this paper.

Ethical approval Not applicable.

Consent to participate Not applicable.

Consent for publication Not applicable.

References

Amalokwu K, Spikes K, Wolf K (2019) A simple effective medium approach for the bulk electrical and elastic properties of organic-rich shales. J Appl Geophys 169:98–108

Archer D (2007) Methane hydrate stability and anthropogenic climate change. Biogeosciences 4(4):521–544

Archie GE (1942) The electrical resistivity log as an aid in determining some reservoir characteristics. Trans AIME 146(01):54–62

Attias E, Amalokwu K, Watts M, Falcon-Suarez IH, North L, Hu GW, Best AI, Weitemeyer K, Minshull TA (2020) Gas hydrate quantification at a pockmark offshore Norway from joint effective medium modelling of resistivity and seismic velocity. Mar Pet Geol 113:104151

Berryman JG (1995) Mixture theories for rock properties. In: Ahrens TJ (ed) Rock physics and phase relations. American Geophysical Union, Washington, pp 205–228

Boswell R, Collett TS (2011) Current perspectives on gas hydrate resources. Energy Environ Sci 4(4):1206–1215

Chand S, Minshull TA, Priest JA, Best AI, Clayton CR, Waite WF (2006) An effective medium inversion algorithm for gas hydrate quantification and its application to laboratory and borehole measurements of gas hydrate-bearing sediments. Geophys J Int 166(2):543–552

Cook AE, Waite WF (2018) Archie's saturation exponent for natural gas hydrate in coarse-grained reservoirs. J Geophys Res: Solid Earth 123(3):2069–2089

Cosenza P, Camerlynck C, Tabbagh A (2003) Differential effective medium schemes for investigating the relationship between high-frequency relative dielectric permittivity and water content of soils. Water Resour Res. https://doi.org/10.1029/2002WR001774

Dugarov GA, Duchkov AA, Duchkov AD, Drobchik AN (2019) Laboratory validation of effective acoustic velocity models for samples bearing hydrates of different type. J Nat Gas Sci Eng 63:38–46

Dvorkin J, Nur A (1996) Elasticity of high-porosity sandstones: Theory for two North Sea data sets. Geophysics 61(5):1363–1370

Ellis M (2008) Joint seismic and electrical measurements of gas hydrates in Countinal Margin sediments. Dissertation, University of Southampton

Fofonoff NP (1985) Physical properties of seawater: A new salinity scale and equation of state for seawater. J Geophys Res: Oceans 90(C2):3332–3342

Gelius LJ, Wang Z (2008) Modelling production caused changes in conductivity for a siliciclastic reservoir: a differential effective medium approach. Geophys Prospect 56(5):677–691

Ghosh R, Ojha M (2021) Amount of gas hydrate estimated from rock physics analysis based on morphology and intrinsic anisotropy in area B, Krishna Godavari offshore basin, expedition NGHP-02. Mar Pet Geol 124:104856

Ghosh R, Sain K, Ojha M (2010) Effective medium modeling of gas hydrate-filled fractures using the sonic log in the Krishna-Godavari basin, offshore eastern India. J Geophys Res: Solid Earth 115(B6):1–15

Goswami BK, Weitemeyer KA, Minshull TA, Sinha MC, Westbrook GK, Chabert A, Henstock TJ, Ker S (2015) A joint electromagnetic and seismic study of an active pockmark within the hydrate stability field at the Vestnesa Ridge, West Svalbard margin. J Geophys Res: Solid Earth 120(10):6797–6822

Haines SS, Collett TS, Yoneda J, Shimoda N, Boswell R, Okinaka N (2022) Gas hydrate saturation estimates, gas hydrate occurrence, and reservoir characteristics based on well log data from the Hydrate-01 Stratigraphic Test Well Alaska North Slope. Energy Fuels 36(6):3040–3050

Han TC (2010) Joint elastic-electrical properties of reservoir sandstones. Dissertation, University of Southampton

Han TC, Best AI, MacGregor LM, Sothcott J, Minshull TA (2011) Joint elastic-electrical effective medium models of reservoir sandstones. Geophys Prospect 59(4):777–786

Han TC, Clennell MB, Cheng ACH, Pervukhina M (2016) Are self-consistent models capable of jointly modeling elastic velocity and electrical conductivity of reservoir sandstones? Geophysics 81(4):D377–D382

Han TC, Yan H, Fu LY, Xu DH (2022) Effective medium modeling of the joint elastic-electrical properties of sandstones with partial water saturation. Geophysics 87(3):MR129–MR137

Helgerud MB, Dvorkin J, Nur A, Sakai A, Collett T (1999) Elastic-wave velocity in marine sediments with gas hydrates Effective Medium Modeling. Geophys Res Lett 26(13):2021–2024

Holland ME, Schultheiss P, Roberts J, Druce M (2008) Observed gas hydrate morphologies in marine sediments. In 6th International Conference on Gas Hydrates, Chevron, Vancouver, BC, Canada (pp. 6–10)

Hu GW, Li CF, Ye YG, Liu CL, Zhang J, Diao SB (2014) Observation of gas hydrate distribution in sediment pore space. Chin J Geophys 57(5):1675–1682

Jakobsen M, Hudson JA, Minshull TA, Singh SC (2000) Elastic properties of hydrate-bearing sediments using effective medium theory. J Geophys Res: Solid Earth 105(B1):561–577

Jensen EH, Gelius LJ, Johansen TA, Wang Z (2013) Consistent joint elastic-electrical differential effective-medium modelling of compacting reservoir sandstones. Geophys Prospect 61(4):788–802

Kvenvolden KA (1993) A primer on gas hydrates: the future of energy gases. US. Geol Surv Prof Pap 1570:279–292

Lee MW (2002) Joint inversion of acoustic and resistivity data for the estimation of gas hydrate concentration. U.S. Geological Survey Bulletin 2190

Lee MW, Collett TS (2009) Gas hydrate saturations estimated from fractured reservoir at Site NGHP-01-10, Krishna-Godavari Basin, India. J Geophys Res: Solid Earth 114(B7):347–358

Lee MW, Collett TS (2012) Pore- and fracture-filling gas hydrate reservoirs in the Gulf of Mexico gas hydrate joint industry project leg II Green Canyon 955 H well. Mar Pet Geol 34(1):62–71

Lee MW, Waite WF (2008) Estimating pore-space gas hydrate saturations from well logacoustic data. Geochemistry Geophysics Geosystems 9(7):1–8

Liu T, Liu XW, Zhu TY (2020) Joint analysis of P-wave velocity and resistivity for morphology identification and quantification of gas hydrate. Mar Pet Geol 112:104036

Markov M, Levine V, Mousatov A, Kazatchenko E (2005) Elastic properties of double-porosity rocks using the differential effective medium model. Geophys Prospect 53(5):733–754

Mavko G, Mukerji T, Dvorkin J (2009) The rock physics handbook. Cambridge University Press, Cambridge

Mukerji T, Berryman JG, Mavko G, Berge PA (1995) Differential effective medium modeling of rock elastic moduli with critical concentration constraints. Geophys Res Lett 22:555–558

Pan HJ, Li HB, Grana D, Zhang Y, Liu TY, Geng C (2019) Quantitative characterization of gas hydrate bearing sediment using elastic-electrical rock physics models. Mar Pet Geol 105:273–283

Pan HJ, Li HB, Chen JY, Riedel M, Holland M, Zhang Y (2020) Cai S (2020) Quantification of gas hydrate saturation and morphology based on a generalized effective medium model. Mar Pet Geol 113:104166

Pandey L, Sain K (2022) Joint inversion of resistivity and sonic logs using gradient descent method for gas hydrate saturation in the Krishna Godavari offshore basin India. Mar Geophys Res 43(3):1–12

Priest JA, Best AI, Clayton CR (2005) A laboratory investigation into the seismic velocities of methane gas hydrate-bearing sand. J Geophys Res: Solid Earth 110(B4):1–13

Ren SR, Liu Y, Liu Y, Zhang W (2010) Acoustic velocity and electrical resistance of hydrate bearing sediments. J Petrol Sci Eng 70(1–2):52–56

Riedel M, Collett TS, Malone M, the Expedition 311 Scientists (2006) Proceedings of the inte-grated ocean drilling program, Volume 311. Integrated Ocean Drilling Program Management International. Inc., Washington, DC.https://doi.org/10.2204/iodp.proc.311.106.200

Riedel M, Goldberg D, Guerin G (2014) Compressional and shear-wave velocities from gas hydrate bearing sediments: examples from the India and Cascadia margins as well as Arctic permafrost regions. Mar Pet Geol 58:292–320

Sava D, Hardage B (2007) Rock-physics models for gas-hydrate systems associated with unconsolidated marine sediments. 77th SEG Technical Program Expanded Abstracts, pp 1579–1583

Sava D, Hardage B, Angelo MD, Murphy P (2011) Evaluating marine gas-hydrate systems. Part II: rock-physics joint inversion of electrical resistivity and seismic velocities. J Seism Explor 20:105–118

Sheng P (1991) Consistent modeling of the electrical and elastic properties of sedimentary rocks. Geophysics 56(8):1236–1243

Sultan N, Cochonat P, Foucher JP, Mienert J (2004) Effect of gas hydrates melting on seafloor slope instability. Mar Geol 213(1–4):379–401

Wu W, Grana D (2017) Integrated petrophysics and rock physics modeling for well log interpretation of elastic, electrical, and petrophysical properties. J Appl Geophys 146:54–66

Yoneda J, Oshima M, Kida M, Kato A, Konno Y, Jin Y, Tenma N (2018) Consolidation and hardening behavior of hydrate-bearing pressure-core sediments recovered from the Krishna-Godavari Basin, offshore India. Mar Pet Geol 118(2019):512–523